Journal of Materials Chemistry A

PAPER

View Article Online
View Journal | View Issue

Cite this: J. Mater. Chem. A, 2016, 4, 7658

Effects of flux synthesis on $SrNbO_2N$ particles for photoelectrochemical water splitting†

Masanori Kodera, Haruki Urabe, Masao Katayama, Takashi Hisatomi, Tsutomu Minegishi and Kazunari Domen*

Received 1st February 2016
Accepted 6th April 2016

DOI: 10.1039/c6ta00971a

www.rsc.org/MaterialsA

An investigation was carried out on the effects of using a flux during the fabrication of $SrNbO_2N$ particles on the photoelectrochemical (PEC) properties of CoPi/$SrNbO_2N$/Nb/Ti photoanodes prepared by a particle transfer method. The type of flux and the synthesis conditions were found to affect the morphology and crystallinity of oxide precursors and subsequently nitrided $SrNbO_2N$. By a suitable choice of flux synthesis conditions, the PEC performance of the photoanodes could be improved. Oxide precursors treated with a NaI flux were solid solutions of $NaNbO_3$ and $Sr_4Nb_2O_9$, and had a perovskite-type structure. When the precursors were first pre-calcined, larger secondary $SrNbO_2N$ particles with a higher degree of crystallinity were obtained. As a result, a photocurrent density of 1.5 mA cm^{-2} at 1.23 V_{RHE} was achieved under simulated sunlight (AM 1.5G) in an alkaline solution (pH 13).

Introduction

Recently, there is increasing awareness that fossil fuels are in danger of becoming depleted and are responsible for global warming.[1] Therefore, the development of new alternative energy sources has become a strong priority. To this end, hydrogen has received a considerable amount of attention as a renewable green fuel, and photoelectrochemical (PEC) water splitting under sunlight is a promising method for clean hydrogen production.[2,3] Among several possible cell configurations, p/n PEC cells consisting of a photoanode and a photocathode are considered to be potential candidates for water splitting without the need for an external bias. In order for this technology to be practical, a solar-to-hydrogen (STH) conversion efficiency of 10% is considered to be a requirement. To achieve this, and assuming that a quantum efficiency (QE) of 60–70% can be obtained in the desired wavelength range, photoelectrodes that can absorb light at wavelengths greater than 600 nm must be used. Thus, the development of photoelectrodes with narrow bandgaps (<2.0 eV) is required.

There have been reports of (oxy)nitrides such as Ta_3N_5 and $LaTiO_2N$, with absorption edges at about 600 nm, both in the form of powder suspensions and as photoelectrodes.[4–7] In particular, perovskite-type oxynitrides with the general formula $AB(O,N)_3$ have been intensively studied.[8,9] In the last several years, reports focusing on Ta-based oxynitrides such as $BaTaO_2N$ have appeared.[10,11] However, there have been few studies on Nb-based perovskite-type oxynitrides, especially for use as photoelectrodes.[12,13] The latter are an attractive material group because their absorption edge is longer than that of other perovskite-type oxynitrides. Furthermore, Nb is more abundant and less expensive than Ta.

$SrNbO_2N$ is a perovskite-type oxynitride with a bandgap of 1.8 eV, and in a powder suspension it can produce both oxygen and hydrogen in the presence of suitable sacrificial reagents.[14,15] Some of the present authors previously reported that $SrNbO_2N$ exhibited n-type semiconducting characteristics and acted as a photoanode in a PEC water splitting cell.[16] Its PEC performance, however, was very low as expected from its wide light absorption range (λ < 700 nm), and it is therefore necessary to improve it. In the previous study, $SrNbO_2N$ particles were synthesized using a polymerized complex technique, and photoanodes were prepared using a particle transfer method.[17] The resulting particles were aggregates of small primary particles with sizes of a few hundred nanometres. The limited photocurrent density of the $SrNbO_2N$ photoelectrodes could be attributed to the low crystallinity of these particles and the electrical resistance at the grain boundaries, which promoted the recombination of the photoexcited carriers. Stability under illumination was another problem for this material. When CoO_x was used as a cocatalyst for water oxidation, the photocurrent rapidly decreased and became almost zero after 10 min at a potential of 1.0 V_{RHE}.

The flux method has been applied to obtain highly crystalline materials. It is widely applied to oxide photocatalysts[18] while there are only few studies on the flux method to oxynitrides and/or their precursors. For example, $La_2Ti_2O_7$ synthesized using an NaCl–KCl flux had high crystallinity, and $LaTiO_2N$ obtained by nitridation of this material exhibited

Department of Chemical System Engineering, School of Engineering, The University of Tokyo, 7-3-1 Hongo, Bunkyo-ku, Tokyo 113-8656, Japan. E-mail: domen@chemsys.t.u-tokyo.ac.jp

† Electronic supplementary information (ESI) available: Additional diffuse reflectance spectra, XRD patterns, TEM images, SEM-EDX measurements and current–potential curves are included. See DOI: 10.1039/c6ta00971a

higher photocatalytic oxygen evolution activity from an Ag^+ containing solution than $LaTiO_2N$ produced using other methods.[6] $BaTaO_2N$ formed by nitriding an oxide precursor in the presence of a KCl flux was shown to have a cubic morphology and excellent crystallinity, resulting in a higher photocatalytic activity than a similar compound produced without a flux treatment.[19] Thus, the flux method is expected to be effective for improving photocatalytic activity by enhancing the crystallinity of particles.

Here, we report the synthesis of $SrNbO_2N$ powder using different types of flux and different flux treatment conditions, and an evaluation of the PEC performance of photoanodes produced using these samples. An investigation was carried out on the effects of using a flux treatment at different stages in the preparation process, the effects of the type of flux, and the effects of pre-calcination on the oxide precursors.

Experimental

Synthesis procedures

(1) Preparation of $SrNbO_2N$ particles with flux treatment at different stages. For flux synthesis of the oxide precursors, an NaCl flux was used. $SrCO_3$, Nb_2O_5, and NaCl were mixed in a molar ratio of Sr : Nb : NaCl = 1 : 1 : 5. The mixture was heated in an alumina crucible for 5 h at 1423 K in air, then cooled to 1073 K at a rate of 1 K min^{-1}, and finally allowed to cool to room temperature. The obtained oxide precursor was then heated for 15 h at 1173 K under an NH_3 flow of 250 mL min^{-1}.

As a flux treatment during nitridation, $SrNbO_2N$ was prepared by the following procedure. A mixture of $SrCO_3$, Nb_2O_5 and NaCl in a molar ratio of Sr : Nb : NaCl = 1 : 1 : 5 in an alumina boat was heated for 15 h at 1173 K under an NH_3 flow of 250 mL min^{-1}, and then cooled to room temperature without interrupting the NH_3 flow. The resulting oxynitride was washed thoroughly with water, filtered, and dried at room temperature.

The third method was a post-nitridation flux treatment of $SrNbO_2N$. About 0.3 g of quartz wool was loaded with a mixture of $SrCO_3$ and Nb_2O_5 in a molar ratio of Sr : Nb = 1 : 1, and heated for 15 h at 1173 K under an NH_3 flow of 250 mL min^{-1} to obtain $SrNbO_2N$. The sample was mixed with a NaCl flux in a molar ratio of $SrNbO_2N$: NaCl = 1 : 5, and heated for 3 h at 1173 K under an NH_3 flow of 250 mL min^{-1} in an alumina boat. The final oxynitride was washed thoroughly with water, filtered, and dried.

As a reference, a $SrNbO_2N$ sample produced without any flux treatment was also prepared. About 0.3 g of quartz wool was loaded with a mixture of $SrCO_3$ and Nb_2O_5 in a molar ratio of Sr : Nb = 1 : 1, and heated for 15 h at 1173 K under an NH_3 flow of 250 mL min^{-1}. In the remainder of this paper, this sample is referred to as SNON (no flux). Similarly, oxynitride samples produced using a flux treatment during oxide synthesis, during nitridation, and the following nitridation are referred to as SNON (oxide), SNON (nitridation), and SNON (post), respectively.

(2) Preparation of SNON (oxide) with various kinds of fluxes. $SrCO_3$, Nb_2O_5, and alkali halide (AX = NaCl, KCl, RbCl, $SrCl_2$, NaBr, KBr, NaI, KI, or CsI) as a flux were mixed in a molar ratio of Sr : Nb : AX = 1 : 1 : 5. The mixture was heated in an alumina crucible for 5 h at 1423 K in air, cooled to 1073 K at a rate of 1 K min^{-1}, and then allowed to cool to room temperature. As a reference, a sample heated without a flux was also prepared. In the nitridation process, the obtained oxide precursors were then heated for 15 h at 1173 K under an NH_3 flow of 250 mL min^{-1}.

The oxide precursors produced without and with a flux, and the resulting nitrided samples are referred to as SNO (no flux), SNO (AX), SNON (no flux) and SNON (AX), respectively.

(3) Preparation of $SrNbO_2N$ particles from SNO (AX) with pre-calcination. In the case of flux treatment of pre-calcined oxide precursors, a mixture of $SrCO_3$ and Nb_2O_5 in a Sr : Nb molar ratio of 1 : 1 was first heated in an alumina crucible for 5 h at 1423 K in air, cooled to 1073 K at a rate of 1 K min^{-1}, and then allowed to cool to room temperature. Subsequently, the product was treated by a flux (NaCl, RbCl, or NaI) using the same procedure as mentioned in (2). In the nitridation process, the oxide was heated for 15–20 h at 1173 or 1223 K under an NH_3 flow of 250 mL min^{-1}.

The pre-calcined oxide precursors and nitrided samples are referred to as SNO (AX, pre-calcined), SNON (AX, pre-calcined).

Characterization

The samples were characterized using X-ray diffraction (XRD; Rigaku, RINT-Ultima III), UV-Vis-NIR diffuse-reflectance spectroscopy (DRS; JASCO, V-670DS), field-emission scanning electron microscopy (FE-SEM; Hitachi, S-4700), and field-emission transmission electron microscopy (FE-TEM; JEOL, JEM-2800). Selected area electron diffraction (SAED) patterns were acquired in the same FE-TEM system. Elemental analysis was performed using inductively coupled plasma atomic emission spectroscopy (ICP-AES; Shimadzu, ICPS-8100), and energy dispersive X-ray spectroscopy (EDX; Horiba, EMAX-7000). To estimate the faradaic efficiency of the $SrNbO_2N$ photoelectrodes under light irradiation, the evolved gases were analysed using micro-gas chromatography (GC; GC3000A, Inficon). Structural parameters were refined by Rietveld analysis using the RIETAN-FP code.[20]

Preparation of $SrNbO_2N$ photoelectrodes

Photoelectrodes were prepared using the particle transfer method.[21] $SrNbO_2N$ powder (30 mg) was dispersed in isopropanol (1 mL). After ultrasonication for more than 5 min, the suspension was deposited dropwise onto a glass plate. Nb and Ti bilayer films were deposited on the samples using a radio-frequency (RF) magnetron sputtering system (ULVAC, MNS-2000-RFG3). A Nb contact layer was first deposited at an RF power of 100 W for 5 min under an Ar pressure of 0.1 Pa. Subsequently, a Ti conductor layer was deposited at an RF power of 200 W for 3 h. The metal layers holding the photocatalyst powder were peeled off and transferred onto another glass plate using carbon tape. Residual particles physically attached to the main particle layer were removed by ultrasonication. Finally, an electrical wire was connected using indium solder, which was then covered with epoxy resin.

Surface modification of photoelectrodes using a CoPi catalyst

Before the PEC measurements, the $SrNbO_2N$ photoelectrodes were loaded with a CoPi cocatalyst by electrodeposition.[22]

$Co(NO_3)_2$ (1 mM) was dissolved in an aqueous solution buffered with 0.1 M potassium phosphate at pH 6.9. The electrode samples were immersed in the electrolyte solution and the electrode potential was held at 1.7 V *vs.* the reversible hydrogen electrode (RHE) for 200 s under darkness to anodically deposit CoPi on the surface of the electrodes.

Photoelectrochemical measurements

PEC measurements were carried out using a three-electrode configuration under intermittent illumination by AM 1.5G simulated sunlight (San'ei Denki, XES-40S2-CE). A Pt wire and an Ag/AgCl electrode were used as the counter and reference electrodes, respectively. The potential was converted into RHE units using the Nernst's equation ($E_{RHE} = E_{Ag/AgCl} + 0.0591 \times pH + 0.199$). The potential was swept from positive to negative at 10 mV s^{-1}. The electrolyte was a 0.2 M aqueous sodium phosphate solution with its pH adjusted to 13 by NaOH addition.

Results and discussion

Flux treatment at different stages

The flux method was used at three different stages: during the synthesis of oxide precursors, nitridation, or post-nitridation treatment of oxynitrides. Fig. 1A shows XRD patterns of nitrided samples produced using an NaCl flux at different stages in the preparation process, together with that of the reference sample for which no flux was used. For all samples, the dominant phase was $SrNbO_2N$. Compared to SNON (no flux), the intensity of the diffraction peaks for all of the flux treated samples increased remarkably, indicating that highly crystalline $SrNbO_2N$ was obtained. The full width at half maximum (FWHM) of the (110) peak for SNON (oxide), SNON (nitridation), and SNON (post) was 0.24, 0.11, and 0.16, respectively, indicating that the crystallinity was improved in the order SNON (oxide), SNON (post), and SNON (nitridation).

The XRD patterns also indicated the presence of an impurity phase of NbO_xN_y (such as $NbO_{0.1}N_{0.9}$, PDF 00-025-1360), except for the case of SNON (oxide). In Fig. S1,† the DRS spectrum of SNON (oxide) is seen to exhibit relatively high background absorption at wavelengths longer than the absorption edge. This can presumably be attributed to anion vacancies and/or reduced Nb species in $SrNbO_2N$ that were produced during nitridation.[17] These results suggest that the presence of nonstoichiometric species cannot be avoided using these flux treatments.

Fig. 1B shows the SEM images of the four different samples. It can be seen that SNON (no flux) and SNON (oxide) both have a porous morphology, similar to that previously reported for $BaTaO_2N$.[10] During nitridation of the oxide precursors, it is thought that many pores are formed as a result of replacing O with N atoms. On the other hand, in the cases of SNON (nitridation) and SNON (post), the surfaces of particles are smooth. The flux treatment during or after nitridation thus promoted crystal growth, resulting in particles with clear crystal habits.

Fig. 1C shows the PEC properties of $SrNbO_2N$ photoelectrodes prepared from the same samples. It can be seen that the flux treatment caused a clear enhancement of the anodic photocurrent, with SNON (oxide) exhibiting the largest photocurrent density. Therefore, a detailed investigation was carried out on the effects of the type of flux used for the oxide precursors on the PEC properties of $SrNbO_2N$.

Effects of the flux type used for oxide precursors

Fig. 2A shows the XRD patterns of oxide precursors prepared with different types of fluxes. It is clear that the type of flux used had an effect on both the crystal structure and the phases that were present. The precursor calcined without a flux was a mixture of $Sr_5Nb_4O_{15}$ and $Sr_2Nb_2O_7$. In contrast, Cl- and Br-based fluxes produced $Sr_2Nb_2O_7$ as the dominant phase. In addition, the use of KCl and RbCl led to the formation of impurity phases such as $KSr_2Nb_3O_{10}$ and $RbSr_2Nb_3O_{10}$, respectively, and a small amount of K or Rb could be detected by SEM-EDX (Table S1†). On the other hand, SNO (NaCl), SNO (NaBr) and SNO ($SrCl_2$) did not contain such impurity phases, although a small amount of $Sr_5Nb_4O_{15}$ was present. In the case

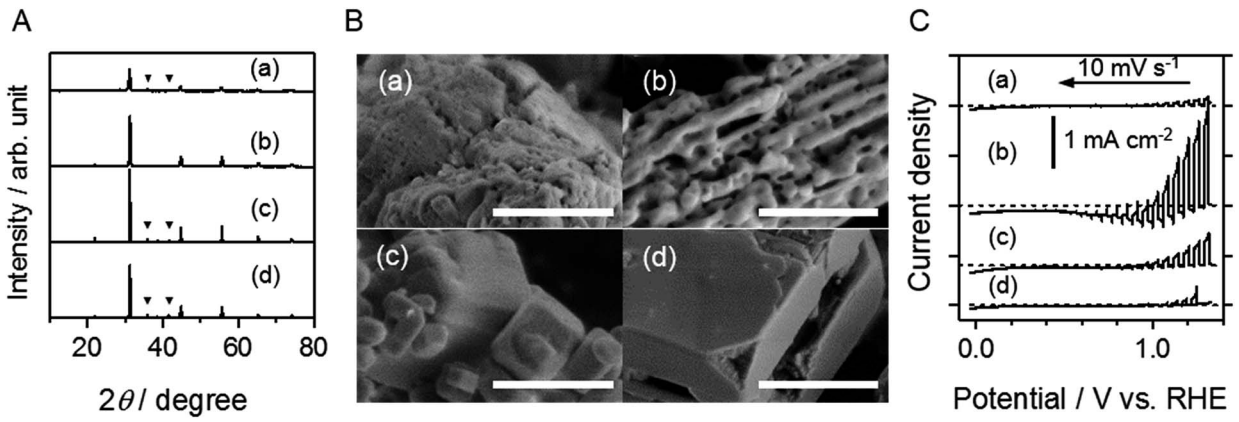

Fig. 1 (A) XRD patterns, (B) SEM images and (C) current–potential curves of $SrNbO_2N$ particles prepared (a) without a flux, and using an NaCl flux (b) during oxide preparation, (c) during nitridation, and (d) following nitridation. The black triangles in the XRD patterns indicate NbO_xN_y. The white bars in the SEM images represent 1 μm. The PEC measurements were performed under AM 1.5G irradiation in 0.2 M Na_3PO_4 with the pH adjusted to 13 by NaOH addition.

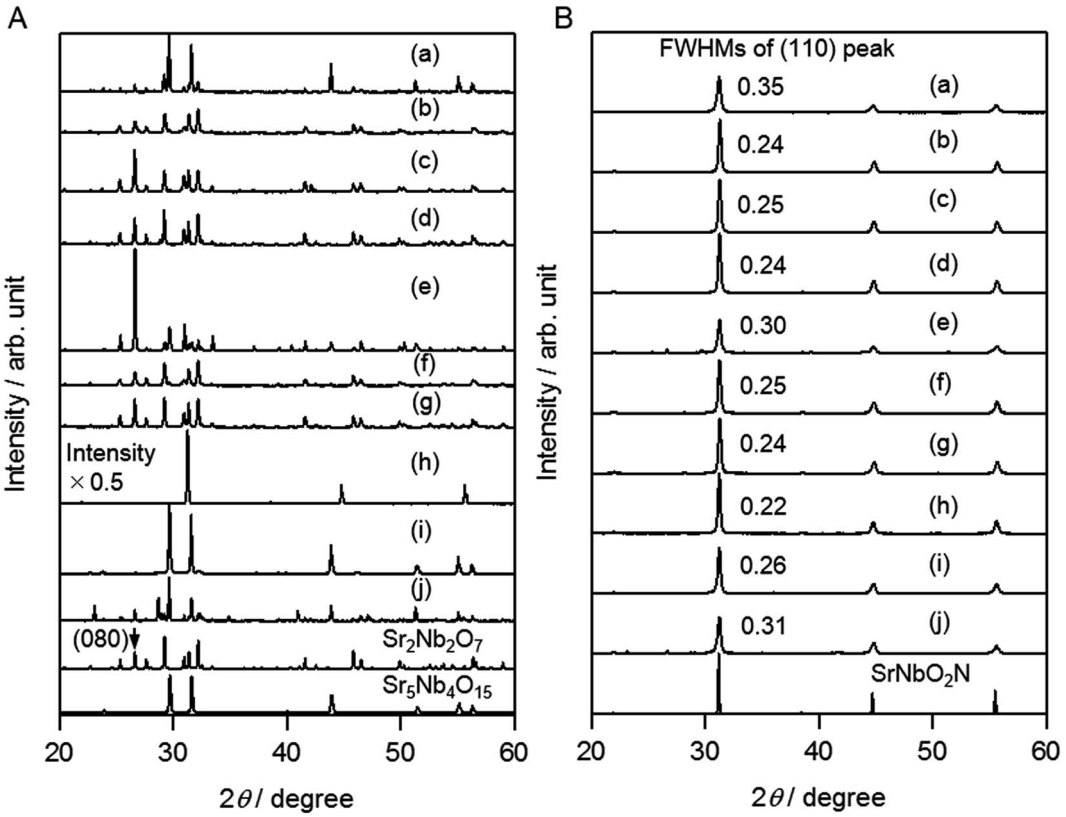

Fig. 2 XRD patterns of (A) oxide precursors and (B) $SrNbO_2N$ particles produced (a) without flux, and with (b) NaCl, (c) KCl, (d) RbCl, (e) $SrCl_2$, (f) NaBr, (g) KBr, (h) NaI, (i) KI, and (j) CsI fluxes. As references, patterns of $Sr_2Nb_2O_7$ (PDF 00-052-0321), $Sr_5Nb_4O_{15}$ (PDF 00-048-0421), and $SrNbO_2N$ (PDF 00-039-0675) are also shown.

of SNO (KI) and SNO (CsI), the dominant phase was $Sr_5Nb_4O_{15}$, but K or Cs containing impurity phases, such as $CsSr_2Nb_3O_{10}$, were identified.

For SNO (NaI), the product was much different from the oxide precursors treated with the other kinds of flux. First, the XRD pattern in Fig. 2A indicates that it has a perovskite-type structure. In addition, in the DRS spectrum in Fig. S2k,† no optical absorption occurs in the visible region. ICP-AES and TEM-EDX measurements were performed to determine the composition of this sample, and the results are shown in Table S2.† It can be seen that a certain amount of Na is present. The nominal composition was determined to be $Na_{0.36}Sr_{0.87}Nb_{0.78}O_3$.

It has been reported that $SrNbO_3$ is a perovskite-type oxide which has a red colour because the valence state of Nb is Nb^{4+}.[23,24] $Na_{(1-x)}Sr_xNbO_3$ also has a perovskite structure, and its colour is from light to deep blue due to the presence of Nb^{4+} species.[25] Based on the DRS results in Fig. S2,† the SNO (NaI) produced in the present study was neither $SrNbO_3$ nor $Na_{(1-x)}Sr_xNbO_3$.

The most likely possibility is that SNO (NaI) is a solid solution of $NaNbO_3$ and $Sr_4Nb_2O_9$. $NaNbO_3$ is a perovskite-type oxide (PDF 01-075-2102), and $Sr_4Nb_2O_9$, which can be denoted as $(Sr(Sr_{1/3}Nb_{2/3})O_3)_3$, is also a perovskite-related oxide (PDF 01-073-9070). Moreover, neither of these compounds exhibit optical absorption in the visible region. Based on the nominal composition determined above for SNO (NaI), the solid solution can be expressed as $(NaNbO_3)_{0.35}$–$(Sr_{4/3}Nb_{2/3}O_3)_{0.65}$. The results of Rietveld refinement based on the solid solution model (see Table S3†) are shown in Fig. 3. Simulated diffraction peaks were well fitted to the experimental ones of SNO (NaI), which offers further support for the presence of a solid solution. Onishi *et al.* also reported a similar solid solution system of $NaTaO_3$ and $Sr_4Ta_2O_9$.[26] The incorporation of Na is thought to occur as follows. During heat treatment at a temperature higher than the melting point of the flux, evaporation will occur to produce AX vapour. In the case of NaI, however, not only NaI but also I_2 vapour is expected to be produced. In fact, a dark purple gas was observed during the flux treatment. As a result, the excess Na^+ is incorporated into the oxide, accompanied by absorption of oxygen from air. SNO (KI) and SNO (CsI) also contained certain amounts of K and Cs, respectively, supporting the above explanation.

The SEM images of oxide precursors prepared with different types of flux are shown in Fig. 4. There is a clear dependence of the morphology on the type of flux used. Without a flux, the particles are generally irregular in shape. In SNO (NaCl), SNO (NaBr), and SNO (RbCl), the particles are column-like, while in SNO (KCl) and SNO (KBr), they are plate-like. In the XRD patterns in Fig. 2A, the relative peak intensities are different for SNO (NaCl) and SNO (KCl). The intensity of the $Sr_2Nb_2O_7$ (080) diffraction peak in SNO (KCl) is much higher than that in SNO (NaCl), which is consistent with the plate-like morphology of

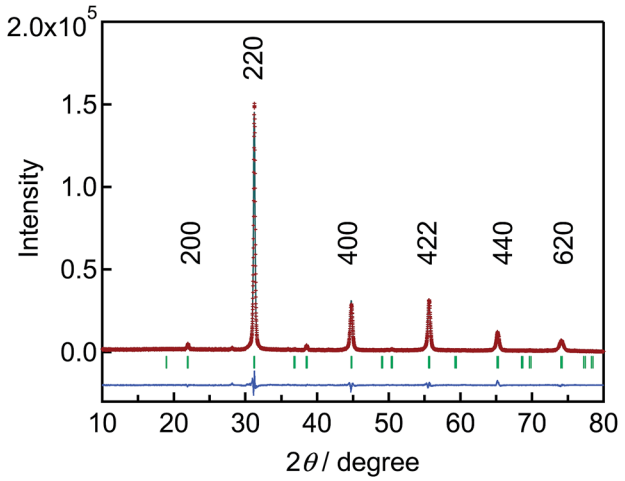

Fig. 3 XRD pattern of SNO (NaI) and the results of Rietveld refinement. The crosses and solid curve represent the observed and calculated patterns, respectively, and the difference between the two is shown at the bottom. The vertical marks indicate the Bragg diffraction positions for $(NaNbO_3)_{0.35}$–$(Sr_{4/3}Nb_{2/3}O_3)_{0.65}$ solid solution. Reliability factors; $R_{WP} = 8.283\%$, $R_B = 1.450\%$.

SNO (KCl) in the SEM images. In SNO ($SrCl_2$), SNO (NaI) and SNO (CsI), relatively large particles were present. Fig. S4† shows TEM images and a SAED pattern of a single secondary SNO (NaI) particle. Clear lattice fringes and diffraction spots are observed, indicating that the particle is most likely a single crystal, which is also consistent with the presence of a solid solution.

As indicated by the XRD results in Fig. 2B, after nitridation of SNO (AX), $SrNbO_2N$ was the main phase in all cases. Compared to the SNON (no flux) sample, the FWHM of the (110) diffraction peak was smaller for all of the SNON (AX) samples, indicating higher crystallinity. For SNON ($SrCl_2$) and SNON (CsI), diffraction peaks associated with the oxide precursors were also observed, suggesting that nitridation was not complete, probably due to large particle size. On the other hand, for SNON (NaI), only diffraction peaks assigned to $SrNbO_2N$ were observed. It should be noted that the ICP-AES analysis revealed that almost all of the Na species in SNO (NaI) evaporated during nitridation (Table S2b†). In addition, as seen in Fig. S2,† a clear absorption edge associated with $SrNbO_2N$ was present. This suggests that SNON (NaI) was completely nitrided, regardless of the relatively large particle size. Thus, nitridation of a perovskite-type oxide precursor to produce a perovskite-type oxynitride without a structural transformation proceeded under relatively mild conditions even when the precursor oxide had large, well crystallized particles. The lattice constants of SNON (no flux) and SNON (AX) refined by Rietveld analysis are shown in Table S4.† No clear trends depending on the type of flux were observed.

The SEM images of SNON (no flux) and SNON (AX) in Fig. S3† show that the morphology of the original oxide precursor particles was maintained in the form of secondary particles after nitridation. The primary particles had sizes on the order of 100 nm regardless of the type of flux.

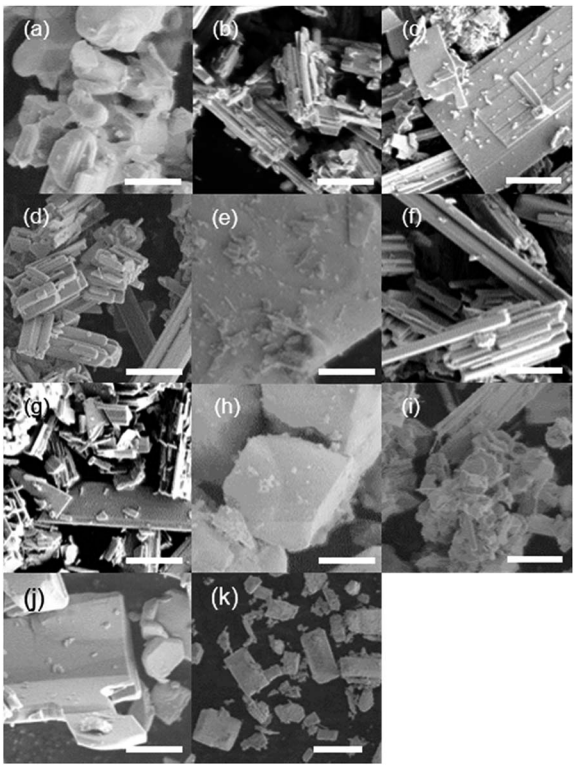

Fig. 4 SEM images of oxide precursors produced (a) without flux, and with (b) NaCl, (c) KCl, (d) RbCl, (e) $SrCl_2$, (f) NaBr, (g) KBr, (h) NaI, (i) KI, (j) CsI, and (k) $SrCl_2$ fluxes. The scale bars in (a)–(j) are 2 μm, and that in (k) is 20 μm.

Fig. 5 shows the PEC properties of the nitrided samples. The photocurrent density of all SNON (AX) samples is seen to be higher than that of SNON (no flux). This is probably due to the higher crystallinity of the primary particles, which results in less recombination of photoexcited carriers in the bulk. Despite the smallest FWHM of SNON (NaI), it did not exhibit the highest photocurrent. One possibility is that other properties such as the morphology or the existence of impurity also affect their PEC performances. At the present stage, these effects are not fully understood. After nitridation, however, most of the flux components evaporated and as a result, less than 1 mol% cation was observed as shown in Table S2.† Thus the effects of doping of cations seem limited. The highest photocurrent density of 1.0 mA cm^{-2} at 1.23 V_{RHE} was obtained for SNON (RbCl), which is more than 1.5 times higher than the previously reported value of 0.6 mA cm^{-2}.[17]

Effects of pre-calcination of the oxide precursor

As discussed above, the flux synthesis of the oxide precursors was found to be effective in improving the PEC properties of the final oxynitrides. In an attempt at further improvement, pre-calcination of the oxide precursors was carried out. The XRD patterns of SNO (AX) and SNO (AX, pre-calcined) are shown in Fig. S5A.† In the case of the NaCl and RbCl fluxes, pre-calcination caused an increase in the intensity of the diffraction peaks for the oxide precursors, indicating an improvement in crystallinity. On the other hand, there was no substantial

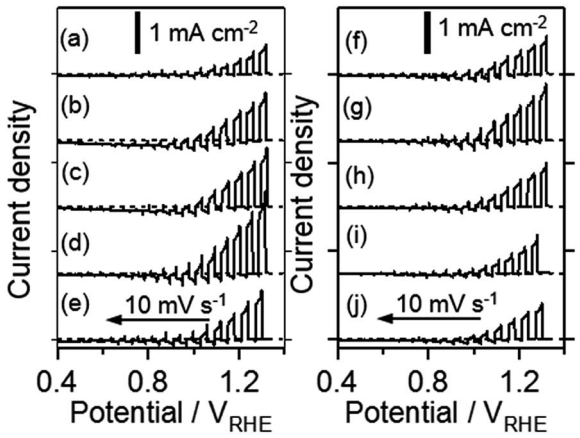

Fig. 5 Current density–potential curves of $SrNbO_2N$ obtained from oxide precursors prepared (a) without flux, and with (b) NaCl, (c) KCl, (d) RbCl, (e) $SrCl_2$, (f) NaBr, (g) KBr, (h) NaI, (i) KI, and (j) CsI fluxes. The PEC measurements were performed under AM 1.5G irradiation in 0.2 M Na_3PO_4 (pH adjusted to 13 by NaOH addition).

difference in the case of NaI. The SEM images of the oxide precursors with and without pre-calcination are shown in Fig. S6.† It can be seen that in all cases, pre-calcination resulted in larger particles.

Fig. S5A† also shows XRD patterns after nitridation of the above oxide precursors. After nitridation for 15 h at 1173 K, oxide diffraction peaks still remained for SNON (NaCl, pre-calcined) and SNON (RbCl, pre-calcined), although the $SrNbO_2N$ phase was dominant. After nitridation for 20 h at 1223 K, both oxide precursors were completely nitrided to $SrNbO_2N$. More severe nitridation conditions were required because of the improvement in the crystallinity of the oxide precursors by pre-calcination. On the other hand, for SNON (NaI, pre-calcined), nitridation for 15 h at 1173 K was enough to obtain single-phase $SrNbO_2N$ even though the particle size became larger by pre-calcination. In addition, nitridation for 20 h at 1223 K seemed to be too severe, resulting in a reduction in the peak intensities.

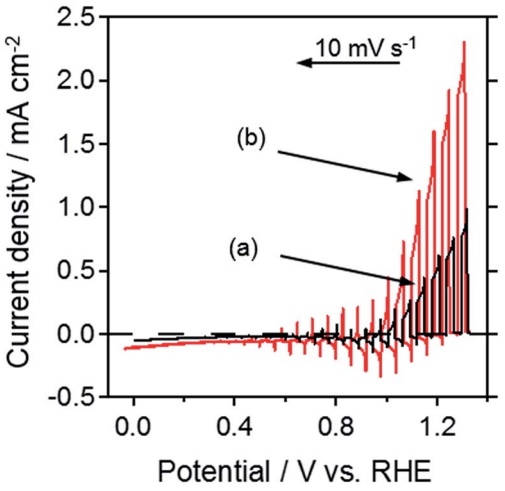

Fig. 6 Current–potential curves of $SrNbO_2N$ prepared from oxide precursors using a NaI flux (a) without pre-calcination, and (b) with pre-calcination, under AM 1.5G irradiation in 0.2 M Na_3PO_4 (pH adjusted to 13 by NaOH addition).

The PEC properties of this series are shown in Fig. 6 and S5.† Regardless of the type of flux, a combination of pre-calcination and appropriate nitridation conditions improved the photocurrent density. In particular, SNON (NaI, pre-calcined) exhibited a value of 1.5 mA cm^{-2} at 1.23 V_{RHE}, which is the highest ever reported for photoanodes fabricated from Nb-based perovskite-type oxynitrides.

The cross-sectional and top-viewed SEM images of SNON (NaI, pre-calcined)/Nb/Ti photoelectrodes are shown in Fig. S7.† Almost a monolayer of secondary particles with sizes of several micrometres is seen to be present on the metal layers. As has been previously proposed, the larger particle size that is possible using the particle transfer method offers advantages in terms of

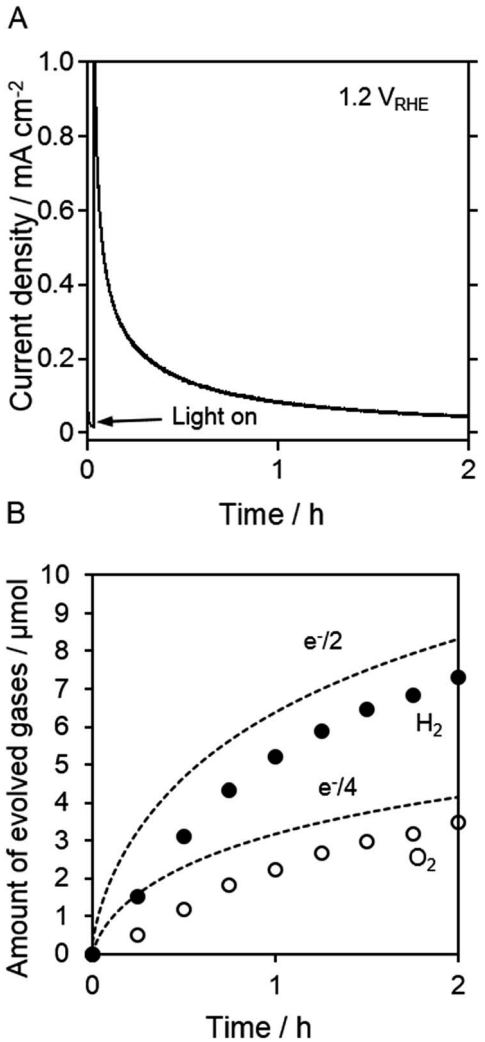

Fig. 7 Time course of (A) photocurrent density and (B) hydrogen and oxygen evolution for $SrNbO_2N$ prepared from pre-calcined oxide precursors using a NaI flux. A voltage of 1.2 V_{RHE} was applied under AM 1.5G irradiation in 0.2 M Na_3PO_4 (pH adjusted to 13 by NaOH addition). The geometric surface area of the electrode was 1.78 cm^2. The dashed lines in (B) indicate estimated amounts of gases from the current–time plot assuming a faradaic efficiency of 100%.

achieving sufficient light absorption.[17] Therefore, the improvement in the PEC properties was considered to be attributed not only to the high crystallinity of the particles, but also to large secondary particles with sizes on the order of micrometres. Moreover, it is likely that the relatively mild nitridation conditions also played a role, partly because the formation of non-stoichiometric species such as Nb^{4+} was suppressed.

Finally, to confirm that the observed anodic photocurrent originated from a water splitting reaction, an analysis of the gas evolved during the reaction was carried out. Fig. 7 shows the time course of the photocurrent density for SNON (NaI, pre-calcined), and of the evolved amount of oxygen and hydrogen. A photocurrent was clearly detected for over 2 h at a potential of 1.2 V_{RHE}. Compared to previous results, the stability of electrodes much improved as well as photocurrent density. It is likely that improved charge transfer decreased the possibility of the occurrence of an undesired reaction such as self-oxidation. As shown in Fig. S8,† surface modification with an appropriate amount of CoPi was effective to improve stability. Moreover, the gases evolved in an almost stoichiometric ratio even though the faradaic efficiency for water oxidation was estimated to be about 80%. This is probably caused by the problem of stirring and self-oxidation. At the initial stage, it takes a certain time until evolved gases become uniform, resulting in the lower faradaic efficiency. At the later stage, self-oxidation seems to play the major role in the reduced faradaic efficiency.

Methods for achieving further improvements in the photocurrent, stability and faradaic efficiency using Nb-based photoanodes are now under investigation.

Conclusions

The effects of flux treatments during the synthesis of $SrNbO_2N$ particles on their PEC properties were investigated. The flux synthesis of oxide precursors improved the photocurrent density, and pre-calcination before the flux treatment further improved the PEC performance. NaI flux-treated $SrNbO_2N$ with pre-calcination exhibited a photocurrent density of 1.5 mA cm^{-2} at 1.23 V_{RHE} under AM 1.5G irradiation.

Acknowledgements

This work was supported in part by Grants-in-Aid for Specially Promoted Research (No. 23000009) and "Nanotechnology Platform" from the Ministry of Education, Culture Sports Science and Technology (MEXT), Japan, and collaboration with Companhia Brasileira de Metalurgia e Mineração (CBMM). The authors would like to acknowledge Dr Taro Yamada at the University of Tokyo for performing the ICP measurements and also acknowledge Dr Yosuke Goto at the University of Tokyo for performing the Rietveld analysis.

References

1 M. Meinshausen, N. Meinshausen, W. Hare, S. C. Raper, K. Frieler, R. Knutti, D. J. Frame and M. R. Allen, *Nature*, 2009, **458**, 1158–1162.
2 N. S. Lewis, *Science*, 2007, **315**, 798–801.
3 L. C. Seitz, Z. Chen, A. J. Forman, B. A. Pinaud, J. D. Benck and T. F. Jaramillo, *ChemSusChem*, 2014, **7**, 1372–1385.
4 E. Nurlaela, S. Ould-Chikh, I. Llorens, J.-L. Hazemann and K. Takanabe, *Chem. Mater.*, 2015, **27**, 5685–5694.
5 J. Seo, T. Takata, M. Nakabayashi, T. Hisatomi, N. Shibata, T. Minegishi and K. Domen, *J. Am. Chem. Soc.*, 2015, **137**, 12780–12783.
6 F. Zhang, A. Yamakata, K. Maeda, Y. Moriya, T. Takata, J. Kubota, K. Teshima, S. Oishi and K. Domen, *J. Am. Chem. Soc.*, 2012, **134**, 8348–8351.
7 M. Matsukawa, R. Ishikawa, T. Hisatomi, Y. Moriya, N. Shibata, J. Kubota, Y. Ikuhara and K. Domen, *Nano Lett.*, 2014, **14**, 1038–1041.
8 J. Xu, C. Pan, T. Takata and K. Domen, *Chem. Commun.*, 2015, **51**, 7191–7194.
9 C. Pan, T. Takata, M. Nakabayashi, T. Matsumoto, N. Shibata, Y. Ikuhara and K. Domen, *Angew. Chem., Int. Ed.*, 2015, **54**, 2858.
10 K. Ueda, T. Minegishi, J. Clune, M. Nakabayashi, T. Hisatomi, H. Nishiyama, M. Katayama, N. Shibata, J. Kubota, T. Yamada and K. Domen, *J. Am. Chem. Soc.*, 2015, **137**, 2227–2230.
11 M. Higashi, Y. Yamanaka, O. Tomita and R. Abe, *APL Mater.*, 2015, **3**, 104418.
12 T. Hisatomi, C. Katayama, K. Teramura, T. Takata, Y. Moriya, T. Minegishi, M. Katayama, H. Nishiyama, T. Yamada and K. Domen, *ChemSusChem*, 2014, **7**, 2016–2021.
13 T. Hisatomi, C. Katayama, Y. Moriya, T. Minegishi, M. Katayama, H. Nishiyama, T. Yamada and K. Domen, *Energy Environ. Sci.*, 2013, **6**, 3595–3599.
14 B. Siritanaratkul, K. Maeda, T. Hisatomi and K. Domen, *ChemSusChem*, 2011, **4**, 74–78.
15 J. Wang, X. Wang, B. Liu, X. Li and M. Cao, *Mater. Lett.*, 2015, **152**, 131–134.
16 K. Maeda, M. Higashi, B. Siritanaratkul, R. Abe and K. Domen, *J. Am. Chem. Soc.*, 2011, **133**, 12334–12337.
17 H. Urabe, T. Hisatomi, T. Minegishi, J. Kubota and K. Domen, *Faraday Discuss.*, 2014, **176**, 213–223.
18 J. Boltersdorf, N. King and P. A. Maggard, *CrystEngComm*, 2015, **17**, 2225–2241.
19 M. Hojamberdiev, K. Yubuta, J. J. M. Vequizo, A. Yamakata, S. Oishi, K. Domen and K. Teshima, *Cryst. Growth Des.*, 2015, **15**, 4663–4671.
20 F. Izumi and K. Momma, *Solid State Phenom.*, 2007, **130**, 15–20.
21 T. Minegishi, N. Nishimura, J. Kubota and K. Domen, *Chem. Sci.*, 2013, **4**, 1120–1124.
22 M. W. Kanan and D. G. Nocera, *Science*, 2008, **321**, 1072–1075.
23 X. Xu, C. Randorn, P. Efstathiou and J. T. Irvine, *Nat. Mater.*, 2012, **11**, 595–598.
24 N. Peng, J. T. Irvine and A. G. Fitzgerald, *J. Mater. Chem.*, 1998, **8**, 1033–1038.
25 B. Ellis, J.-P. Doumerc, M. Pouchard and P. Hagenmuller, *Mater. Res. Bull.*, 1984, **19**, 1237–1243.
26 L. An and H. Onishi, *ACS Catal.*, 2015, **5**, 3196–3206.

